

**Composition-Dependent Structural and Gradually Tunable Bandgap of
GeS_{1-x}Se_x Alloys Synthesized via Chemical Vapor Transport**

Der-Yuh Lin^a, Feng-Hsing Chou^a, Shang-Wei Chen^a, Sin-Wei Huang^b, Yu-Tai Shih^b,
and Shih-Yu Huang^{b*}

^a Department of Electronic Engineering, National Changhua University of Education,
Changhua 500208, Taiwan, ROC.

^b Department of Physics, National Changhua University of Education, Changhua
500207, Taiwan, ROC.

***To whom all correspondence should be addressed**

Prof. Shih-Yu Huang

E-mail address: syhuang@cc.ncue.edu.tw (S.-Y. Huang)

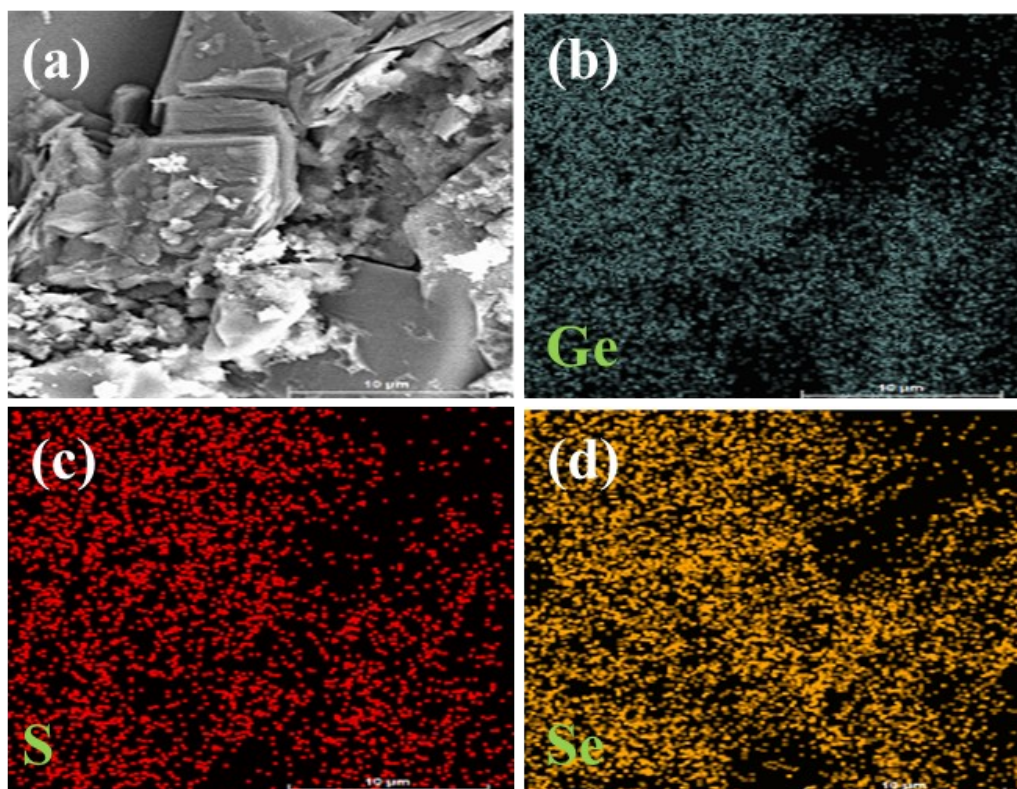


Fig. S1. (a) SEM image of the $\text{GeS}_{0.39}\text{Se}_{0.61}$ sample and their corresponding EDX elemental mapping of (b) Ge, (c) S, and (d) Se, respectively.

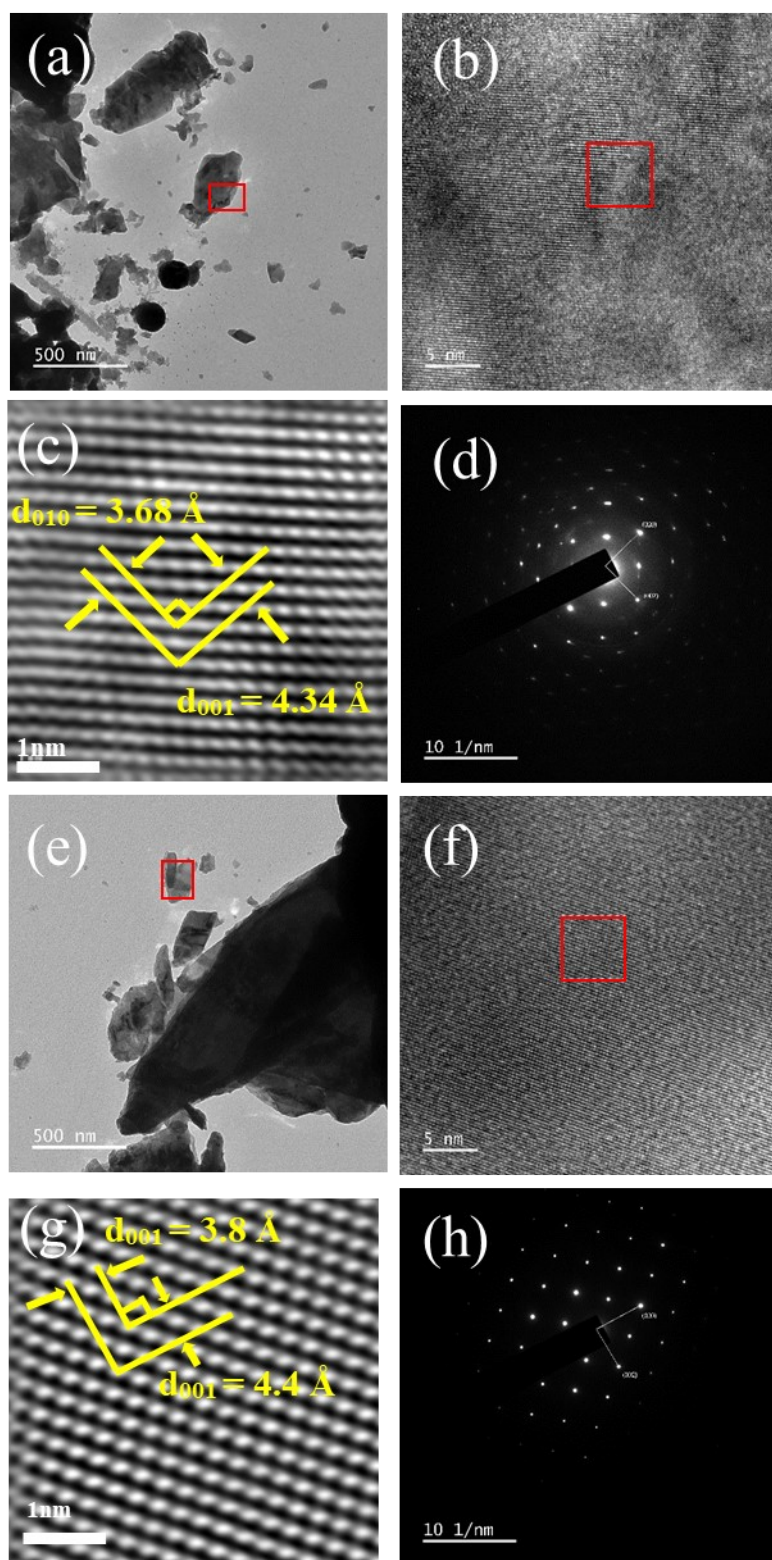


Fig. S2. TEM and HR-TEM images along with their corresponding inverse fast Fourier transform (IFFT) and SAED patterns of (a–d) $\text{GeS}_{0.79}\text{Se}_{0.21}$, (e–h) $\text{GeS}_{0.15}\text{Se}_{0.85}$.

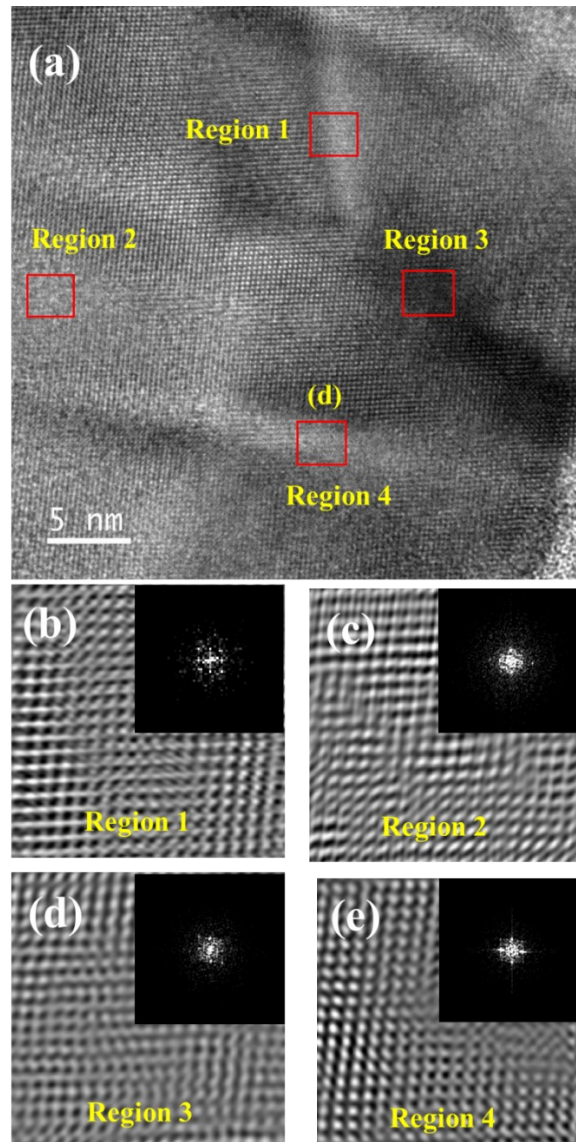


Fig. S3. (a) HRTEM image of the GeS_{0.39}Se_{0.61} alloy. (b–e) The IFFT images and the corresponding FFT patterns of regions 1–4.

All selected regions, together with their corresponding SAED (FFT) patterns, exhibit discrete diffraction spots rather than diffuse halo rings, confirming the preservation of long-range crystallinity. The IFFT images in specific regions reflect lattice deformation, indicative of a highly strain-disordered crystalline structure with interfacial lattice deformation. This clarification reinforces that the observed strain relaxation arises from defect accumulation and interfacial distortion within a crystalline framework.

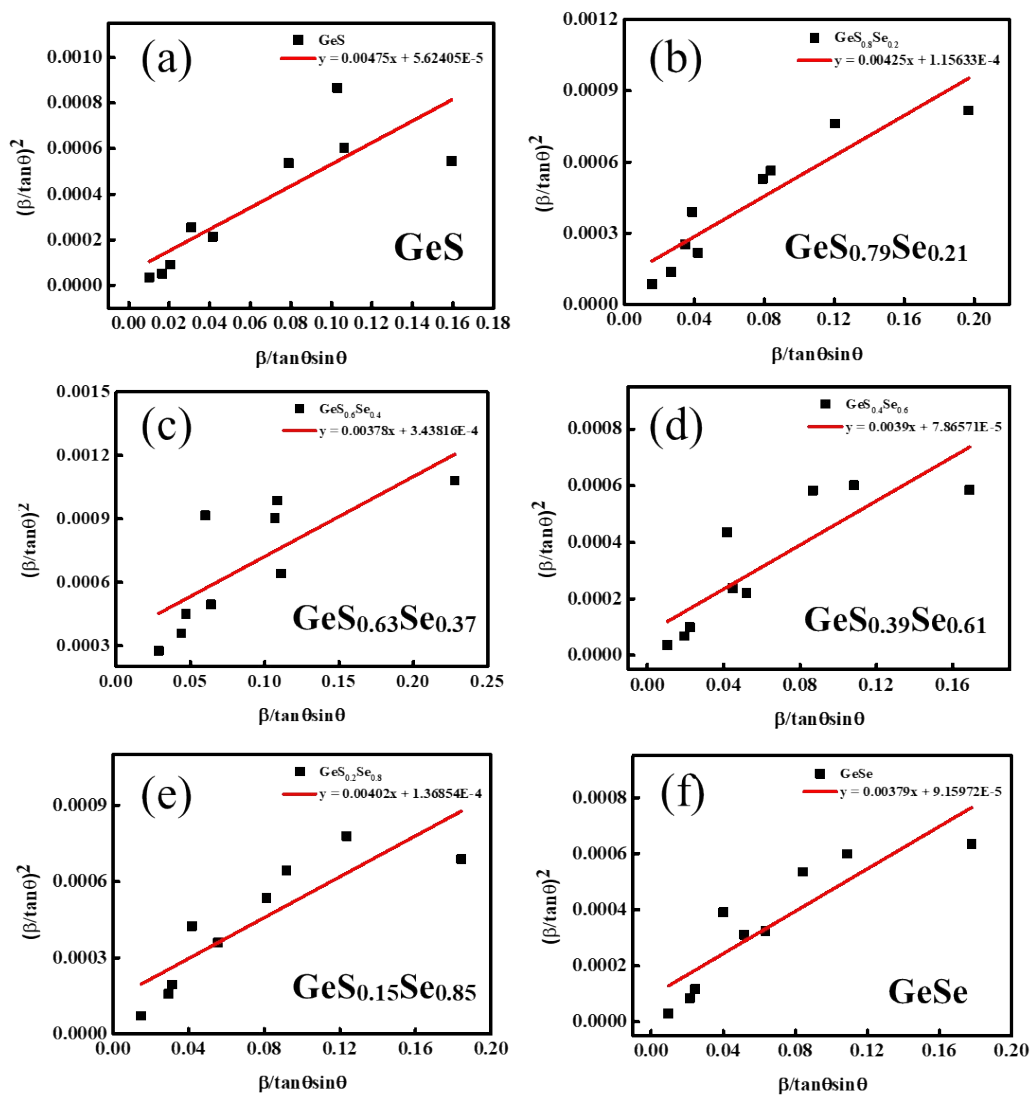


Fig. S4. Graphs of Halder–Wagner for estimating the crystallite sizes and strains of (a) GeS, (b) $\text{GeS}_{0.79}\text{Se}_{0.21}$, (c) $\text{GeS}_{0.63}\text{Se}_{0.37}$, (d) $\text{GeS}_{0.39}\text{Se}_{0.61}$, (e) $\text{GeS}_{0.15}\text{Se}_{0.85}$, and (f) GeSe.

According to Hooke's law, the deformation energy density for a given crystallographic

plane (hkl) can be expressed as: [1]

$$\mu_{hkl} = \frac{\varepsilon^2 Y_{hkl}}{2} \quad (1)$$

Therefore, the total deformation energy density can be written as:

$$\sum \mu_{hkl} = \sum \frac{\varepsilon^2 Y_{hkl}}{2} \quad (2)$$

Where μ_{hkl} is lattice deformation energy density, h, k, and l are the Miller indices of the reflecting plane, Y_{hkl} is the direction-dependent Young's modulus. For the orthorhombic $\text{GeS}_{1-x}\text{Se}_x$ alloy, Y_{hkl} can be calculated using the elastic compliance constants S_{ij} as follows the reference reported by Gomes et. al: [2]

$$\frac{1}{Y_{hkl}} = \frac{S_{11}h^4 + S_{22}k^4 + S_{33}l^4 + (2S_{12} + S_{66})h^2k^2 + (2S_{13} + S_{55})h^2l^2 + (2S_{23} + S_{44})k^2l^2}{(h^2 + k^2 + l^2)^2} \quad (3)$$

And ε is the strain value from Williamson–Hall model:

$$\beta \cos \theta = \frac{K\lambda}{D} + 4\varepsilon \sin \theta$$

where β is the corrected full width at half maximum (FWHM, in radians), θ is the Bragg angle, D is the crystallite size, ε is the strain value, K is the Scherrer constant (typically ~ 0.9), and λ (1.5418\AA) is the X-ray wavelength.

Assuming that the Young's modulus follows a linear composition dependence (Vegard's law), we have:[3]

$$Y_{hkl} = (1-x)Y_{hkl}^{\text{GeS}} + xY_{hkl}^{\text{GeSe}} \quad (4)$$

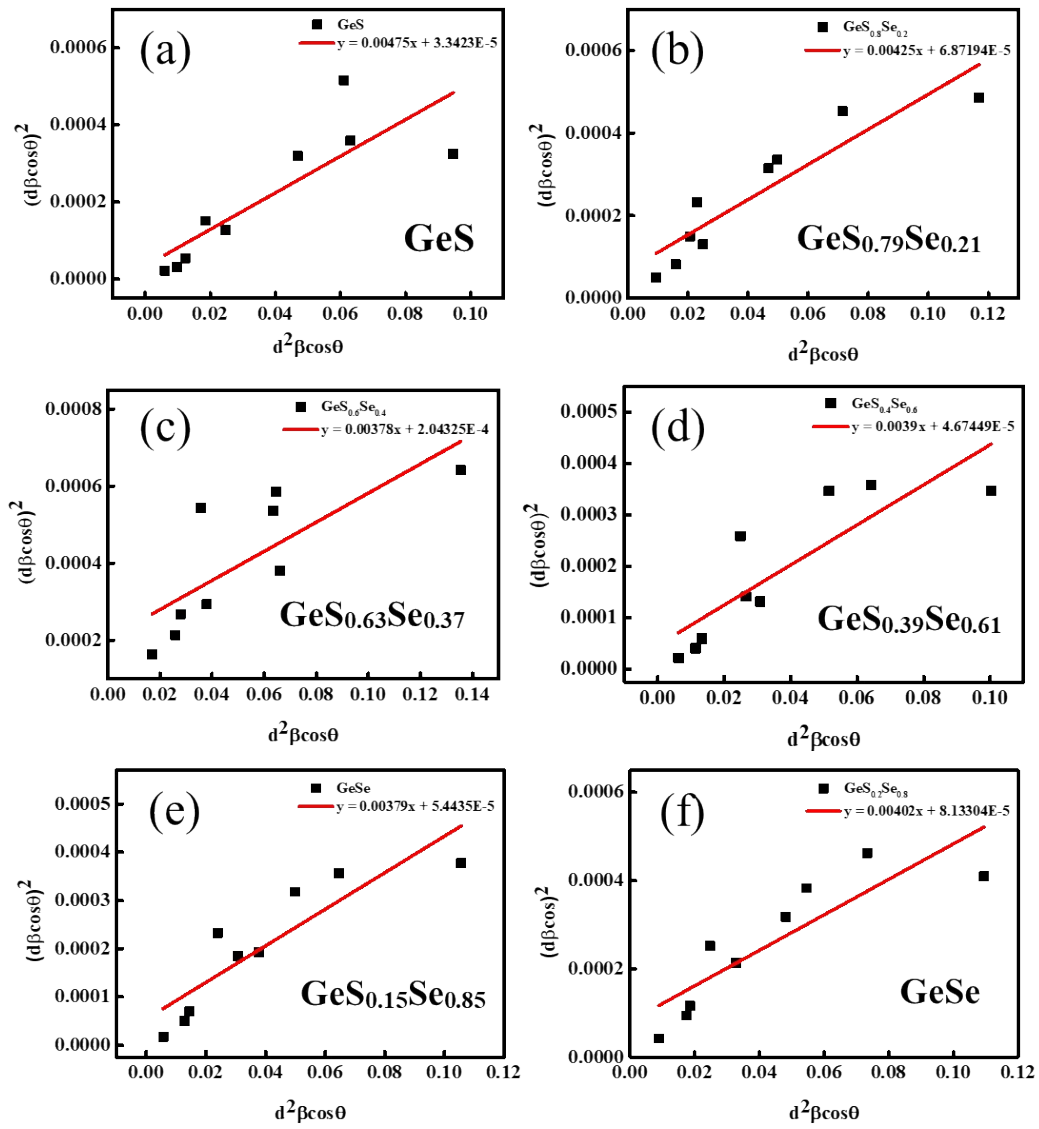


Fig. S5. Graphs of Size-Strain Plot for estimating the crystallite sizes and strains of (a) GeS, (b) $\text{GeS}_{0.79}\text{Se}_{0.21}$, (c) $\text{GeS}_{0.63}\text{Se}_{0.37}$, (d) $\text{GeS}_{0.39}\text{Se}_{0.61}$, (e) $\text{GeS}_{0.15}\text{Se}_{0.85}$, and (f) GeSe.

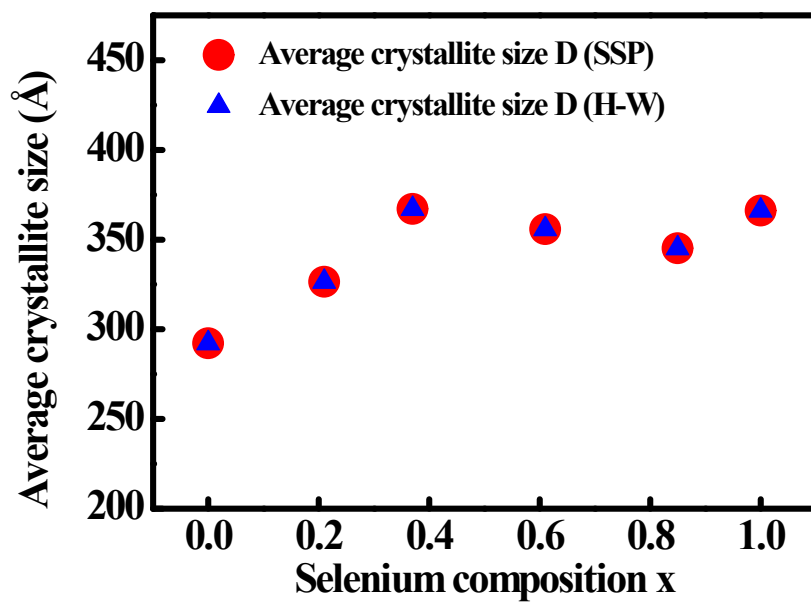


Fig. S6. Variation of crystallite size (D) of $\text{GeS}_{1-x}\text{Se}_x$ alloys as a function of selenium composition (x), estimated using the H–W and SSP methods.

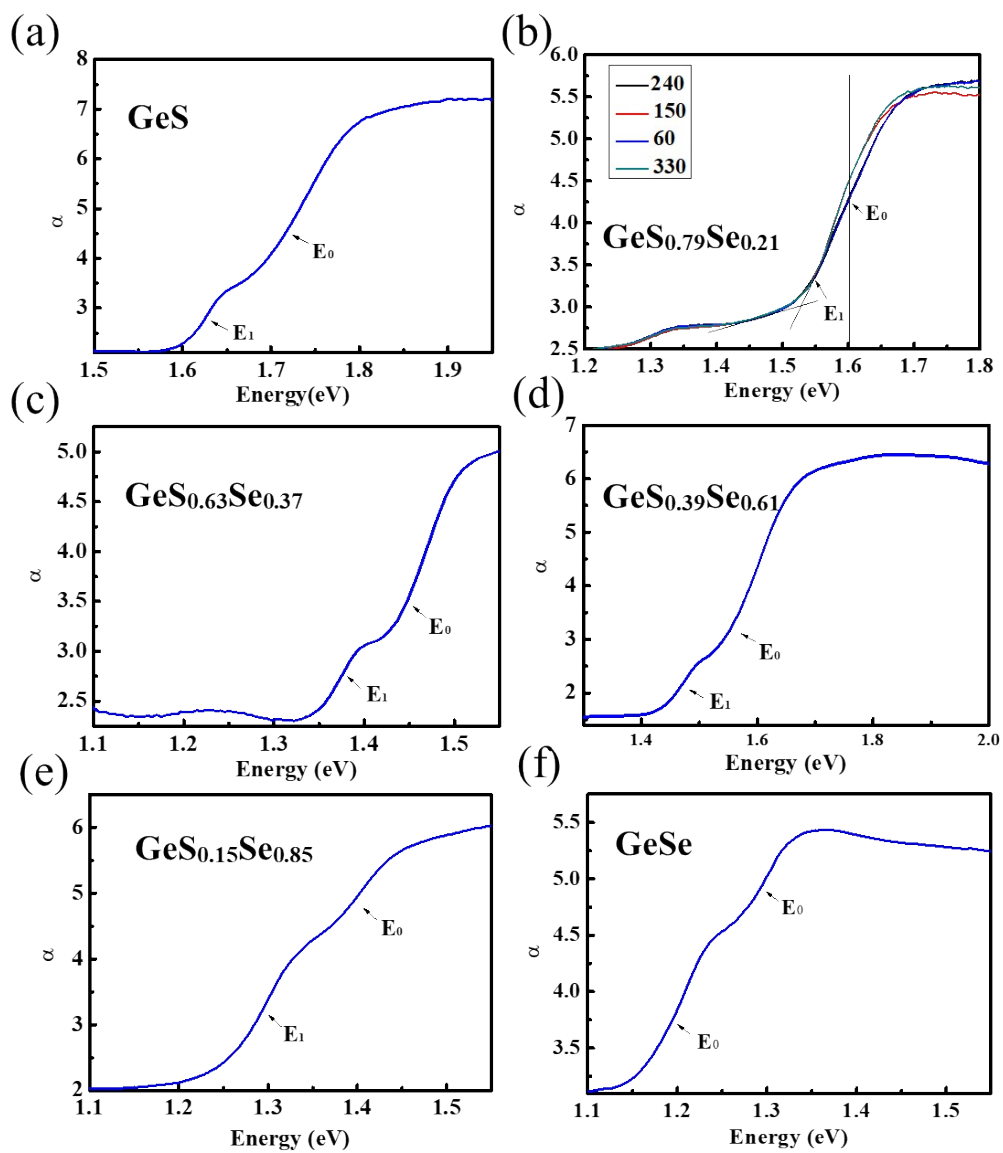


Fig. S7. The optical absorption spectra of $\text{GeS}_{1-x}\text{Se}_x$ alloys with various Se contents: (a) GeS, (b) $\text{GeS}_{0.79}\text{Se}_{0.21}$, (c) $\text{GeS}_{0.63}\text{Se}_{0.37}$, (d) $\text{GeS}_{0.39}\text{Se}_{0.61}$, (e) $\text{GeS}_{0.15}\text{Se}_{0.85}$, and (f) GeSe sample.

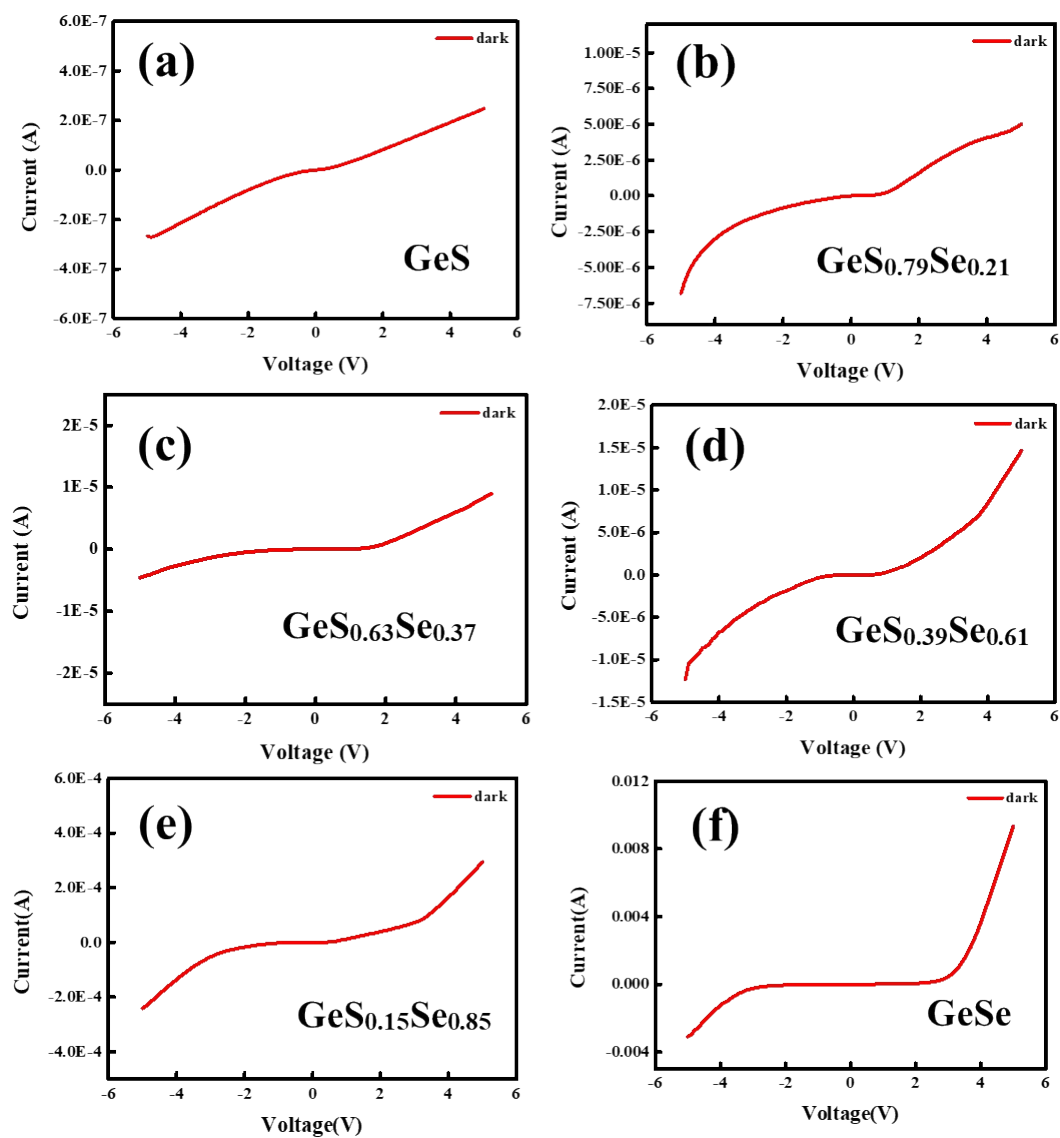


Fig. S8. Current–voltage (I–V) characteristics of $\text{GeS}_{1-x}\text{Se}_x$ alloys: (a) GeS, (b) $\text{GeS}_{0.79}\text{Se}_{0.21}$, (c) $\text{GeS}_{0.63}\text{Se}_{0.37}$, (d) $\text{GeS}_{0.39}\text{Se}_{0.61}$, (e) $\text{GeS}_{0.15}\text{Se}_{0.85}$, and (f) GeSe sample.

Reference:

- [1] M.K. Alam, M.S. Hossain, N.M. Bahadur, S. Ahmed, A comparative study in estimating of crystallite sizes of synthesized and natural hydroxyapatites using Scherrer Method, Williamson-Hall model, Size-Strain Plot and Halder-Wagner Method, *J. Mol. Struct.* 1306 (2024).
<https://doi.org/10.1016/j.molstruc.2024.137820>.
- [2] L.C. Gomes, A. Carvalho, A.H. Castro Neto, Enhanced piezoelectricity and modified dielectric screening of two-dimensional group-IV monochalcogenides, *Phys. Rev. B Condens. Matter Mater. Phys.* 92 (2015) 1–9.
<https://doi.org/10.1103/PhysRevB.92.214103>.
- [3] F. Iori, S. Ossicini, R. Rurali, Structural and electronic properties of Si_{1-x}Gex alloy nanowires, *J. Appl. Phys.* 116 (2014). <https://doi.org/10.1063/1.4898130>.